Original Article

Ridge operator-assisted delineation of capsulorhexis border for cataract surgery

Yishan Li[1], Xiaogang Wang[2], Qiong Gong[1], Minghui Deng[3], Shuchao Chen[1], Hongbo Chen[1]

[1]School of Life & Environmental Science, Guangxi Colleges and Universities Key Laboratory of Biomedical Sensors and Intelligent Instruments, Guilin University of Electronic Technology, Guilin, China; [2]Department of Cataract, Shanxi Eye Hospital Affiliated to Shanxi Medical University, Taiyuan, China; [3]Department of Cataract, Linfen Yaodu Eye Hospital, Linfen, China

Contributions: (I) Conception and design: Y Li, S Chen, H Chen; (II) Administrative support: H Chen, X Wang; (III) Provision of study materials or patients: X Wang, Q Gong, M Deng, H Chen; (IV) Collection and assembly of data: X Wang, M Deng; (V) Data analysis and interpretation: Y Li, S Chen, X Wang; (VI) Manuscript writing: All authors; (VII) Final approval of manuscript: All authors.

Correspondence to: Hongbo Chen, PhD. School of Life & Environmental Science, Guangxi Colleges and Universities Key Laboratory of Biomedical Sensors and Intelligent Instruments, Guilin University of Electronic Technology, No. 1 Jinji Road, Guilin 541004, China. Email: hongbochen@163.com; Xiaogang Wang, MD, PhD. Department of Cataract, Shanxi Eye Hospital Affiliated to Shanxi Medical University, No. 100 Fudong Street, Taiyuan 030001, China. Email: wangxiaogang@sxmu.edu.cn.

Background: With the continuous development of machine vision and imaging technology and its application in computer-aided diagnosis, it is clinically important to use computer technology to assist physicians in accurate cataract surgery. The capsulorhexis directly affects the outcome of cataract surgery, therefore, we design a method to automatically determine the virtual boundary of capsulorhexis for cataract surgery planning and tracking *in-vivo* to help surgeons achieve a more ideal capsulotomy geometry.

Methods: In this study, an effective method was proposed to detect and display the location of capsulorhexis in cataract videos *in-vivo*. The initial step was locating the entire eye area by analyzing the connected components of the mirror reflective points in the image in the cataract surgery video. Then, an operator was designed for ridge edge variation and used to extract pupil edge features. Lastly, circular Hough transform was used to detect the pupillary margin and calculate the boundary between the scleral limbus and the virtual capsulorhexis border in accordance with the pupillary margin and finally displayed it *in-vivo* during cataract surgery.

Results: The method was tested on eight videos of cataract surgery and the results showed that 98.52% accuracy was achieved in the localization of the specular reflection point. We compared the proposed operator with the Sobel, Scharr, Laplace and Canny operators and the results showed that our operator achieved the smallest mean square error with the greatest structural similarity.

Conclusions: The analysis demonstrated that the proposed operator outperformed other operators in detection and achieved satisfactory results in the videos of actual cataract surgeries.

Keywords: Continuous curvilinear capsulorhexis; pupillary margin; ridge edge; cataract video; cataract surgery planning

Submitted Nov 26, 2022. Accepted for publication May 05, 2023. Published online May 25, 2023.
doi: 10.21037/qims-22-1319
View this article at: https://dx.doi.org/10.21037/qims-22-1319

Introduction

Continuous curvilinear capsulorhexis (CCC) is a very important step in cataract surgery (1-3). A good continuous circumferential capsulotomy directly affects the outcome of cataract surgery and the best postoperative refractive outcome (4). Too large or too small capsulorhexis could increase the risk of posterior capsular opacity (5-7). During cataract surgery, capsulorhexis is performed by a cataract surgeon with the use of forceps to create an opening in the capsule, approximately 4.0–5.8 mm in diameter, on the anterior surface of the lens capsule of the human eye (5,6). In the process of capsulorhexis, the position of the capsulorhexis needs to be judged by the surgeon on the basis of experience, which increases the difficulty of the surgeon's actual operation (7). Therefore, the use of edge extraction technology to assist in surgery could effectively improve the accuracy of CCC and the success rate of the surgery.

Circular corneal markers and a limbus-centered capsulotomy mark have emerged during the development of capsulotomy to optimize the capsular tear (8-10). Although the reference ring marking increases the accuracy of the capsulorhexis procedure, placing the reference ring increases not only the complexity of the procedure but also the risk of unexpected intraoperative problems (7). To this end, a simple capsulorhexis virtual boundary generation method based on the cataract surgery video was designed in accordance with the characteristics of pupil edge changes during cataract surgery.

However, most of the current methods for image edge detection could only detect the step edge and ramp edge, and the operator has difficulty at detecting the ridge edge (11-18). As cataract is an invasive surgery, the destruction of the ocular edge by the instruments greatly increases the difficulty of edge detection.

Figure 1 shows the changes in different positions of the pupil edge in the grayscale image. In the enlarged image, an obvious boundary could be seen at the pupil edge position. In the three-dimensional (3D) image corresponding to each position, an obvious gray gradient change could be found at the edge of the eye, and the gradient changes into a ridge shape. Therefore, a ridge operator was designed in accordance with the edge change. First, the entire eye position was located using the reflective point. After the initial interception of the eye position by intraoperative localization points, the image edge was extracted using the ridge operator. Finally, the tear capsule opening, pupillary margin, and scleral limbus positions were detected and displayed *in-vivo* by Hough transform.

Methods

As shown in *Figure 2*, the method was divided into two steps of specular reflection point location and boundary delineation. In the first step, the cataract surgery video was inputted as a frame image, and the image was cropped by locating the specular reflection points in the image as the input for feature extraction. In the second step, the edge feature of the pupil edge of the eyeball was extracted using the ridge operator, and the position of the pupil edge circle was calculated in accordance with the edge feature. After each frame of image was processed to delineation the edge and outline the virtual boundary, the processed image was outputted in the form of video in sequential frames to complete the detection and tracking of the pupil edge in cataract surgery.

Materials

The cataract surgery video data used in this study came from Shanxi Provincial Eye Hospital, and a total of eight cases were obtained from real-shot videos during clinical cataract surgery. In accordance with the analysis and decomposition of intraoperative cataract video, a total of 3,600 CCC images of cataract were selected for testing, and the size of each image was 576×720 pixels.

Primary location

Due to the non-uniformity of the recording equipment used in cataract surgery, the sizes and specifications of various cataract surgery videos differ. Specular reflections are caused by the illumination used for image acquisition, and they appear as brightest points in the iris region of eye images. A method of using specular reflection points to initially locate and intercept the eye area was adopted to overcome the size difference caused by video recording.

The input cataract surgery color image of size 576×720×3 was converted to grayscale, and Gaussian filtering was selected to process the image to reduce high-frequency noise. Mathematical morphological operations (19) select appropriate structural elements to act on the image and process and perform certain operations to meet the requirements.

After the filtered image was binarized with a fixed

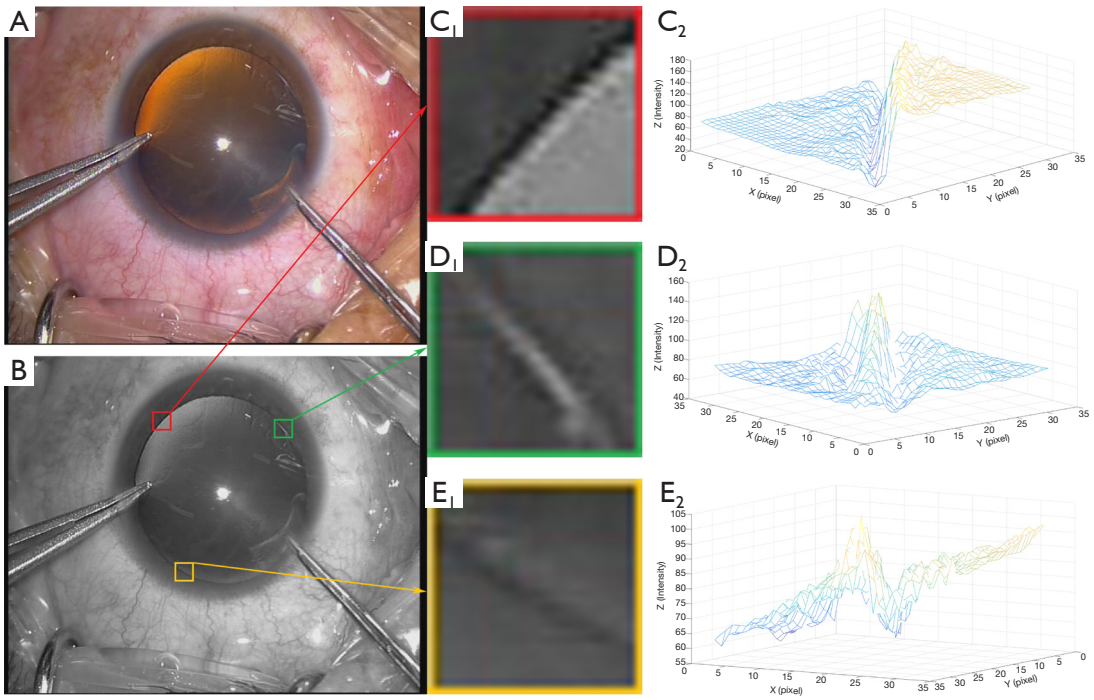

Figure 1 Gradient change in pupil edge. (A) The original cataract surgery image; (B) the grayscale change image of (A); (C_1,D_1,E_1) the magnified images of the pupil edge information in the grayscale image; (C_2,D_2,E_2) the three-dimensional gradient magic figures of C_1, D_1, and E_1, respectively.

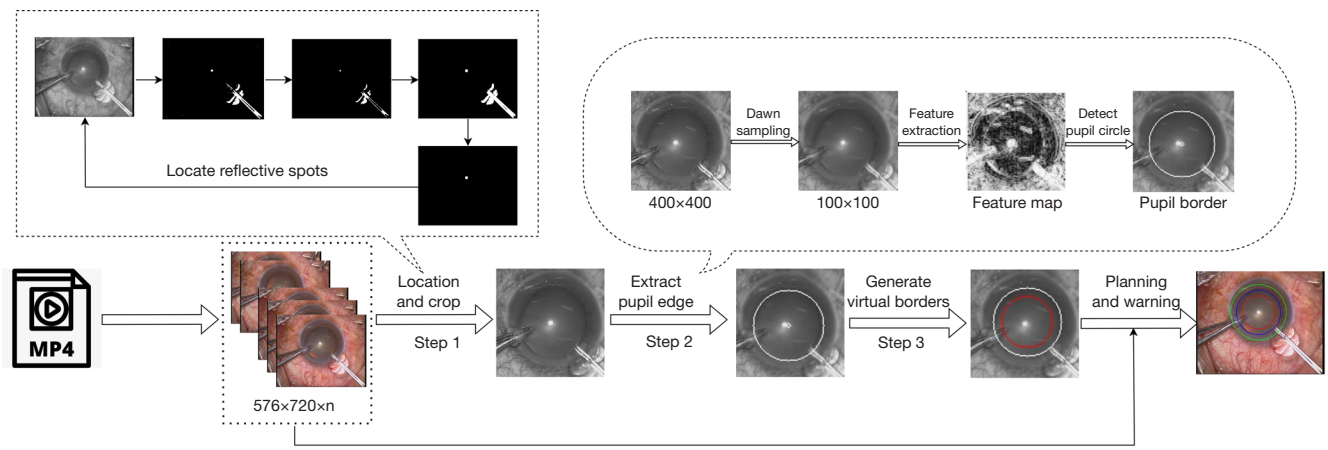

Figure 2 Virtual capsulorhexis border detection and tracking process in cataract surgery.

threshold, a series of dilation and erosion was used to clean up small spots in the binary image and re-grow the remaining areas. The pixel count threshold was set to determine reflective spots. In the image with a size of 576×720 pixels, the connected area with the number of pixels between 250 and 600 was selected as the target bright area, and the minimum closed circle of the bright area was calculated. The center of the smallest closed circle was taken as the specular reflection point, and a rectangular area of 400×400 pixels was selected, with the specular reflection

point as the center as the eyeball area, for preliminary positioning and interception.

Border detection

In calculus, the first derivative of a one-dimensional function is defined as follows:

$$\frac{\mathrm{d}f}{\mathrm{d}x}=\lim_{\varepsilon\to 0}\frac{f(x+\varepsilon)-f(x)}{\varepsilon} \quad [1]$$

The image is treated as a two-dimensional function $f(x,y)$, defined by partial differential as:

$$\frac{\partial f(x,y)}{\partial x}=\lim_{\varepsilon\to 0}\frac{f(x+\varepsilon,y)-f(x,y)}{\varepsilon} \quad [2]$$

$$\frac{\partial f(x,y)}{\partial \mathrm{y}}=\lim_{\varepsilon\to 0}\frac{f(x,y+\varepsilon)-f(x,y)}{\varepsilon} \quad [3]$$

As the image is a one-dimensional discrete function, the minimum interpolation between pixels is 1, so ε=1 is substituted into the above formula to obtain:

$$\frac{\partial f(x,y)}{\partial x}=f(x+1,y)-f(x,y)=g(x) \quad [4]$$

$$\frac{\partial f(x,y)}{\partial \mathrm{y}}=f(x,y+1)-f(x,y)=g(\mathrm{y}) \quad [5]$$

Through a 3×3 operator matrix, the image intensity gradient at each point of the image was calculated by sliding, and the edge features in the horizontal and vertical directions of the image could be obtained.

In a real eye image, the pupillary margin presents an obvious ridge in the grayscale image. Therefore, in a 3×3 operator matrix, its edge features could be highlighted by weighing the eigenvalues of the ridge position pixels. The operator is $f(x,y)$ to calculate the partial derivative of the 3×3 neighborhood at the center of four directions of *x, y, xy, yx*. A certain weight was added to the center point of the operator to reduce the noise in the eye image. The digital gradient approximation equation of the operator could be described as follows:

$$\begin{aligned}G_x=&\left[f(x-1,y-1)+f(x-1,y+1)+f(x+1,y-1)+f(x+1,y+1)\right]\\&+2\left[f(x,y-1)+f(x,y+1)\right]\\&-2\left[f(x-1,y)+2f(x,y)+f(x+1,y)\right]\end{aligned} \quad [6]$$

$$\begin{aligned}G_y=&\left[f(x-1,y-1)+f(x-1,y+1)+f(x+1,y-1)+f(x+1,y+1)\right]\\&+2\left[f(x-1,y)+f(x+1,y)\right]\\&-2\left[f(x,y-1)+2f(x,y)+f(x,y+1)\right]\end{aligned} \quad [7]$$

$$\begin{aligned}G_{xy}=&\left[f(x-1,y)+f(x+1,y)+f(x,y-1)+f(x,y+1)\right]\\&+2\left[f(x-1,y+1)+f(x+1,y-1)\right]\\&-2\left[f(x-1,y-1)+2f(x,y)+f(x+1,y+1)\right]\end{aligned} \quad [8]$$

$$\begin{aligned}G_{yx}=&\left[f(x-1,y)+f(x+1,y)+f(x,y-1)+f(x,y+1)\right]\\&+2\left[f(x-1,y-1)+f(x+1,y+1)\right]\\&-2\left[f(x-1,y+1)+2f(x,y)+f(x+1,y-1)\right]\end{aligned} \quad [9]$$

The computation matrices with such edge features is given as follows:

$$\Delta x=\begin{vmatrix}1&2&1\\-2&-4&-2\\1&2&1\end{vmatrix} \quad [10]$$

$$\Delta y=\begin{vmatrix}1&-2&1\\2&-4&2\\1&-2&1\end{vmatrix} \quad [11]$$

$$\Delta xy=\begin{vmatrix}-2&1&2\\1&-4&1\\2&1&-2\end{vmatrix} \quad [12]$$

$$\Delta yx=\begin{vmatrix}2&1&-2\\1&-4&1\\-2&1&2\end{vmatrix} \quad [13]$$

where Δx and Δy represent the ridge edge features in the horizontal and vertical directions, respectively, and Δxy and Δyx represent the ridge edge features in the 45° and 135° oblique directions, respectively.

The image was obtained by sliding the above operator matrices pixel by pixel to obtain the characteristics of the four directions in accordance with the formula:

$$G(x,y)=\max\left(|G_x|,|G_y|,|G_{xy}|,|G_{yx}|\right) \quad [14]$$

By using $G(x,y)$ to obtain the edge features of the image. After the extracted edge feature image was normalized and equalized, the approximate circle of the pupil edge was extracted by Hough transform (8,20-22). In accordance with the position of the center of the pupillary margin, an

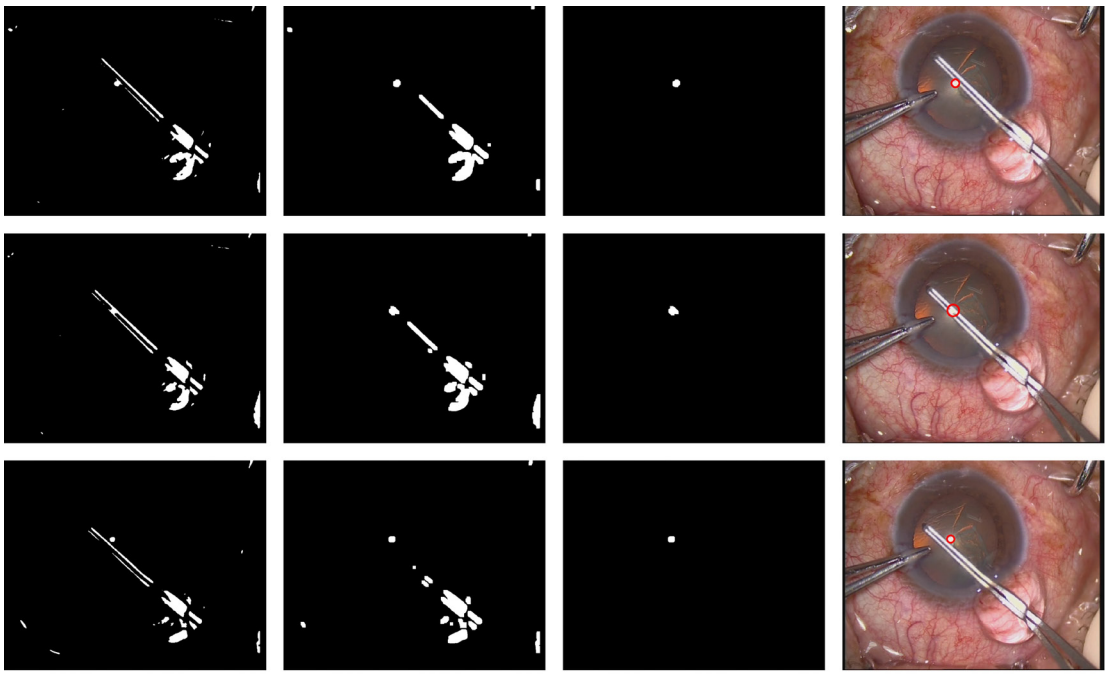

Figure 3 Localization result of capsulorhexis forceps occluding the specular reflection point. The threshold image shows the filtered and denoised original image. Character image shows the feature map obtained by erosion and dilation of the image in the first column. Filter image shows the results after connected component filtering. Result image shows the minimum circle drawn on the third image, which is displayed on the original image.

approximate circle of the virtual capsulorhexis border and the scleral limbus was drawn in the image.

Results

In this paper, an algorithm for pupillary margin detection and tracking in cataract surgery was proposed. The experiment used Intel (R) Core (TM) i9-9900K CPU @ 3.60GHz Central processing unit, and the operating environment is Windows 10.

Location result of reflection point

In the specular reflection point positioning scheme proposed in this paper, corrosion and expansion were used to reduce the reflection of the surgical film and water, and the influence of the displacement and deformation of the reflection point caused by the movement of the instruments during the operation was suppressed. *Figure 3* shows the results of locating the specular point when capsulorhexis tweezers occlude the specular point.

The coordinates of the center of the specular reflection point in cataract surgery were marked in the normal environment and in the environment with more severe light interference and compared without corrosion expansion and without primary selection. The Euclidean distance between the prediction result and the manual marking result was taken as the judging standard, the artificial marking point as the center of the circle, and a circle with a distance of 8 pixels as the judging area to calculate the accuracy of the predicted specular reflection point falling within the judging area.

As shown in *Table 1*, the proposed method achieved an accuracy of 0.9981 under normal light conditions. The average error was only 1.6995-pixel units due to the fact that the interference of small light spots is eliminated after corrosion expansion, and the target area was enlarged at the same time. In another case images with severe environmental interference, the proposed method could still achieve an accuracy of 0.9852. Moreover, the average error in the images with severe environmental interference was only 2.0226-pixel units.

Table 1 Influence of different situations on results

Method	Normal image		Interfere image	
	Distance (pixels)	Accuracy	Distance (pixels)	Accuracy
Without erode and dilate	16.8242	0.7515	36.0092	0.6314
Without primary selection	6.9822	0.9845	216.4371	0.2352
Proposed method	1.6995	0.9981	2.0226	0.9852

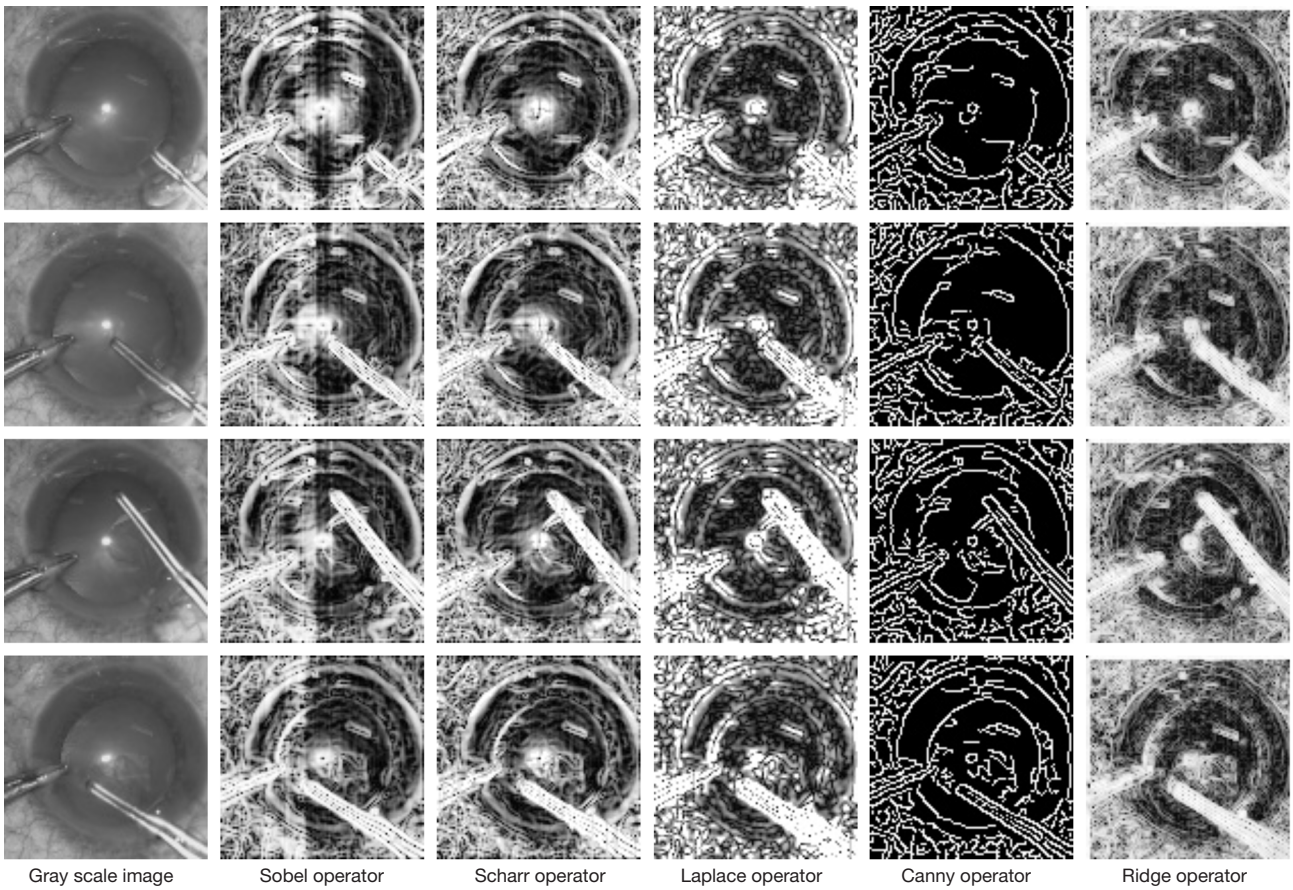

Figure 4 Pupillary margin features extracted by different operators. The leftmost column shows the grayscale image of the original image. Each of the remaining columns displays the edge extraction results obtained using different operators on the grayscale image on the left. The Sobel, Scharr, Laplace, Canny, and proposed ridge operators were utilized for edge extraction.

Result comparison in different feature extraction operators

In this paper, the feature map was used to detect the image edges by using the ridge operator. The proposed method was compared with five different edge detection algorithms of Sobel, Scharr, Laplace, and Canny, and the result is shown in *Figure 4*.

Considering Sobel and Scharr operators are step-type edge extraction operators, they are very poor for ocular ridge-shaped edge extraction, and the feature extraction process is interfered by the light that presents step-type changes. For Laplace and Canny operators, although the ocular ridge-shaped edge could be extracted, pupil edge extraction is difficult to perform because of the interference between the fundus vessels and light in the feature map. Meanwhile, the proposed operator could effectively extract the completed pupil rim edge while overcoming the noise.

Table 2 Results of applying the edge detection operator to pupil edge image

Variables	Sobel	Scharr	Laplace	Canny	Ridge
MSE (mean ± SD)	1,927±524	1,782±546	2,424±827	6,600±1,296	1,613±481
SSIM (mean ± SD)	0.66±0.04	0.66±0.04	0.64±0.05	0.67±0.04	0.68±0.05
PSNR (mean ± SD)	15.43±1.15	15.82±1.33	14.54±1.48	10.02±0.82	16.24±1.29

MSE, mean square error; SSIM, structural similarity; PSNR, peak signal-to-noise ratio; SD, standard deviation.

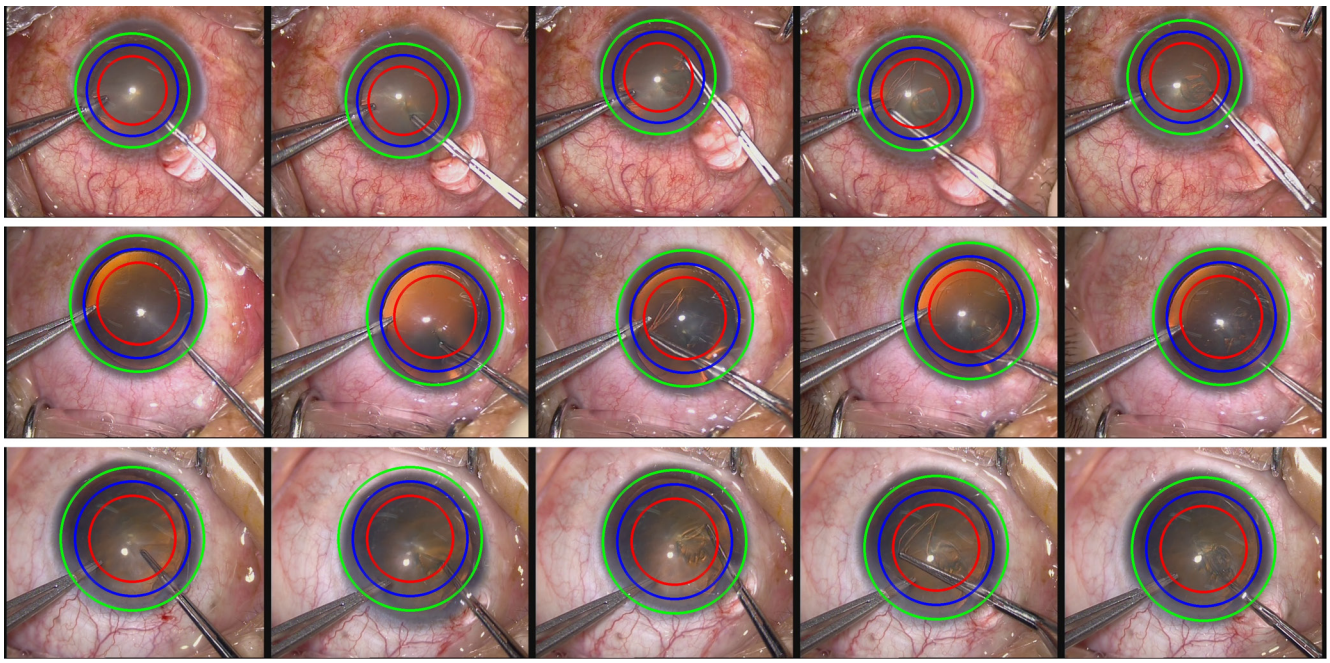

Figure 5 Illustration of some key frames. The blue circle represents the pupillary margin, the green circle represents the scleral limbus, and the red circle represents the virtual capsulorhexis border.

In the actual cataract surgery video, the scleral limbus, pupillary margin, and virtual capsulorhexis border were sequentially extracted by the proposed method to reflect the ability of the operator to extract the ridge edge. The structural similarity and peak signal-to-noise ratio between the scleral limbus and capsulorhexis region of each image and the ground truth image of the scleral limbus and capsulorhexis region were calculated. Three cases of cataract surgery videos were selected. Then, the images in which the scleral limbus, pupillary margin, and virtual capsulorhexis border were successfully detected were selected for comparison, and the average value and corresponding deviation of the detection results of each frame of images were counted. The results are shown in *Table 2*.

As shown in *Table 2*, in the error between the image extracted by the contrast operator and the real ground image, the feature map extracted by the ridge operator has the smallest mean square error with the real ground image and the largest structural similarity performance and peak signal-to-noise ratio. This finding indicates that for the pupil edge feature, the edge extracted by the ridge operator has higher similarity with the pupil edge and less noise and distortion.

Results of cataract surgery video

The coordinates of the specular reflection point were reserved from the second frame on the basis of the Euclidean distance between the frames to further utilize the information between the frames before and after the video. *Figure 5* shows the final performance of the proposed algorithm on actual surgical videos.

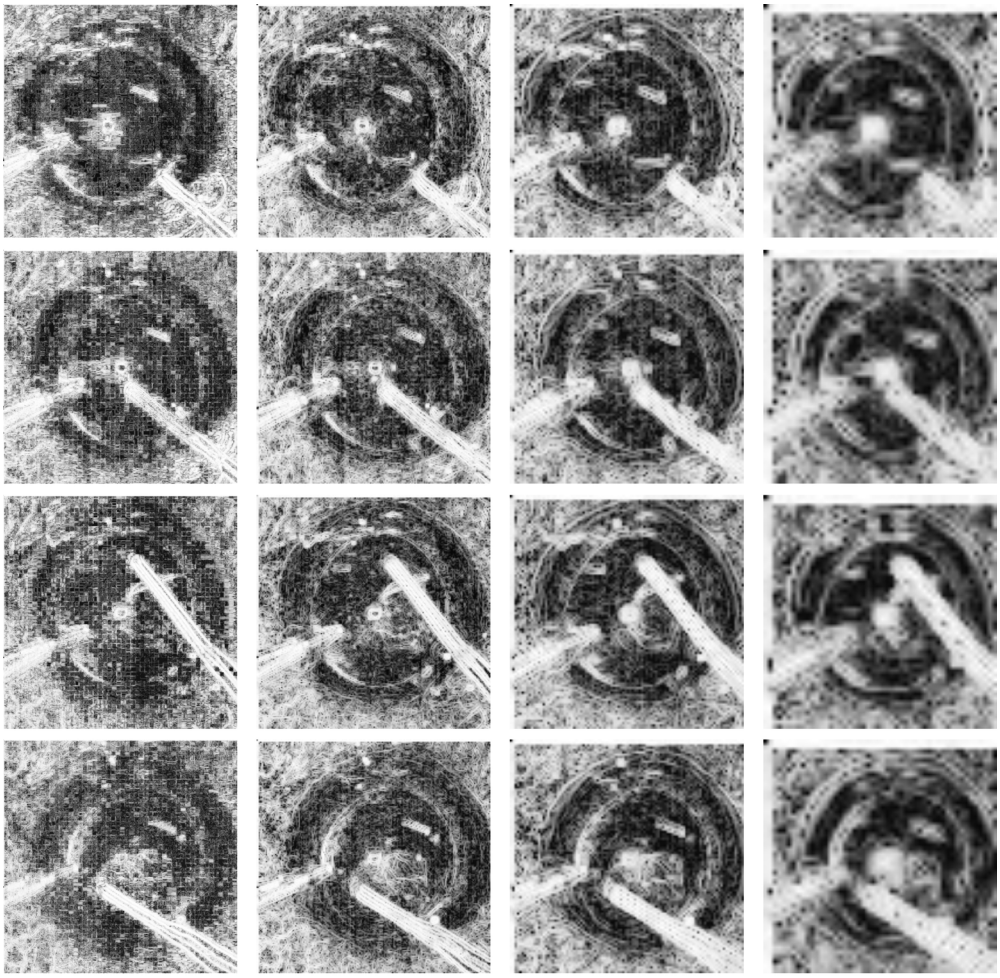

Figure 6 Extraction effect of feature maps of different sizes.

Result of pupillary margin extraction

In the process of edge feature extraction on the grayscale image after positioning and cropping, the image needs to be down-sampled first. As shown in *Figure 6*, edge feature extraction was carried out under the original feature map, one sampling, two samplings, and three samplings. The results showed that the effect of feature extraction is best in the case of two down-samplings. Given that in the images of cataract surgery videos, the boundary of the pupil edge of the eye is gradually transitioned, in the 3×3 operator field of view, the effect of slowly transitioning feature extraction could be worse. Therefore, the down-sampling method was used to improve the signal-to-noise ratio and receptive field to obtain a clearer boundary. However, in excessive down-sampling, the image could lose its original information and features. The experiments in this work proved that using 100×100 feature maps for pupil edge feature extraction could achieve the best results, which are not only obtaining a clear pupil edge boundary but also retaining more information in the image.

After the image features were extracted by the ridge operator, the pupil edge was extracted by Hough transform. The effect was tested under different surgical cases, as shown in *Figure* 7. In the test, eight actual cases of cataract surgery provided by Shanxi Eye Hospital were selected, and the images at the beginning of the intraoperative capsulorhexis were chosen. The feature map was normalized and equalized after positioning, the edge features were cut and extracted to improve the features of the edge of the pupil, and the Hough circle transform was used to detect this edge.

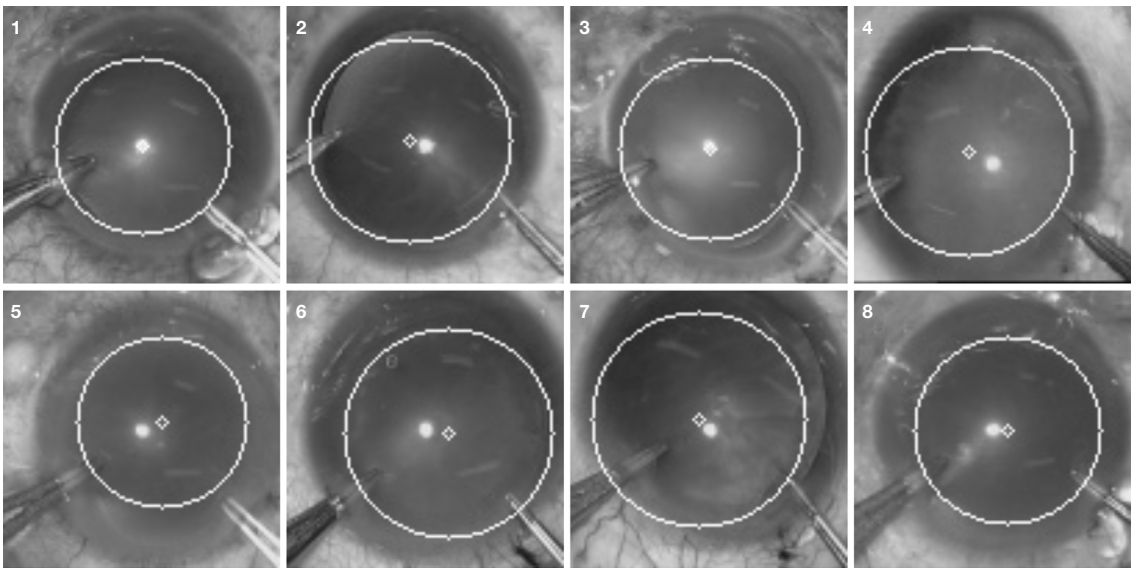

Figure 7 Pupil edge extraction results of different cases.

In cataract surgery videos, individual differences could affect the results. In procedures with more standard procedures, brighter fundus lights could show more obvious edges in the image. However, when the light is insufficient and the patient's lens nucleus is opaque, the edge of the fundus is more blurred, and the extracted pupil edge could be slightly deviated.

In-vivo analysis

In this paper, Python was chosen as the programming language to examine the *in-vivo* performance in actual cataract surgery videos. The algorithm was accelerated using CPU parallel computing. On Intel® Core™ i9-9900K CPU @ 3.60GHz platform, with 16 threads parallelism in Python3.7 environment, the algorithm could achieve 14.02 frames per second (FPS). The variation was analyzed in the variance of each image frame in the cataract surgery video, and slight image variation was found in the 3–5 consecutive frames of the video. One frame was taken in every three frames in the video for calculation to ensure the accuracy of the program and improve the smoothness, and the final result could reach 42.05 FPS. The experimental results satisfy the requirement of *in-vivo*.

Discussion

In this paper, a method of eye boundary delineation and tracking in cataract surgery was proposed, and a ridge operator was designed in accordance with the characteristics of intraoperative pupil boundary changes. The experimental results show that in the actual cataract surgery images, the ridge operator could highlight the edge features of the pupillary margin more obviously, and its effect is better than that of Sobel, Scharr, Laplace, and Canny operators. By using the features of the pupil edge, the virtual boundaries of the pupillary margin, the scleral limbus, and the capsulorhexis could be drawn *in-vivo* in continuous cataract surgery videos.

In the practical application of the proposed method, the specular reflection point was used to locate the eyeball, the target area was initially intercepted, and two down-samplings were performed to simplify the calculation amount and improve the running speed of the program to meet the *in-vivo* performance in cataract surgery videos. The edge of the pupil was extracted by the ridge operator, the optimal position of the capsulorhexis of the eyeball was calculated in accordance with the pupil edge, and the virtual boundary of the position of the capsulorhexis was displayed *in-vivo* during the operation. The algorithm was tested to run at 42.05 FPS. The source code for the algorithm could be found on https://github.com/finallfish/Capsulorhexis-Virtual-Border. The proposed method could assist surgeon to complete capsulorhexis surgery and provide technical support for subsequent cataract surgery.

By combining these improvements with the tracking

process, our method offers a more reliable and effective approach for analyzing cataract surgery videos. The use of information between adjacent frames, along with the saved position information of the specular reflection point, helps to reduce errors in the labeling process. Furthermore, manually measuring the diameter of the pupillary margin in the first frame allows for more precise and efficient tracking of its position, resulting in a more accurate use of the Hough transform to locate the pupillary margin circle. Together, these enhancements provide a powerful tool for the analysis of cataract surgery videos.

The method proposed in this paper could efficiently extract the pupillary margin and scleral limbus by using the specular reflection point and the ridge operator. Moreover, the virtual boundaries of the pupillary margin, the scleral limbus, and the capsulorhexis border could be drawn *in-vivo* in cataract surgery videos. However, in the actual operation process, as the surgical instrument could squeeze the eyeball during the operation, the position of the virtual capsulorhexis could be affected when the eyeball is greatly deformed. In addition, this method is only aimed at eyeball boundary recognition in cataract surgery videos, and its effect on eyeball boundary extraction in other ophthalmic surgeries is unclear. In the follow-up work, the method should be tested for the extraction of eyeball boundaries in other ophthalmic surgeries, and the scheme should be improved on the basis of the problems identified.

Conclusions

We have proposed a new method for tracking the capsulorhexis boundary in cataract surgery using surgery video, where the boundary has been determined by the pupil margin. Additionally, we have designed a ridge edge extraction operator to effectively extract the ridge edge changes in the image. To assist surgeon in surgery without additional invading the eyeball, we have also proposed an *in-vivo* planning, tracking scheme for cataract surgery. Together, these contributions have offered a promising approach for improving the safety and effectiveness of cataract surgery.

In the future work, based on the virtual boundaries of the pupillary margin, scleral limbus and capsulorhexis that have been detected by this method, combined with other intraoperative positioning and tracking methods, the surgeon's intraoperative operations will be monitored and early warnings will be given where problems may occur. This can assist the surgeon to complete the operation better.

Acknowledgments

Funding: This work was supported by the National Natural Science Foundation of China (Grant Nos. 82260358 and 81971697), research funding from Shanxi Eye Hospital (No. B201804), the Shanxi Scholarship Council of China Grant (No. 2021-174 to X Wang). The above-mentioned funding sources had no role in the design of this study, during its execution, analyses, interpretation of the data, or decision to submit results.

Footnote

Conflicts of Interest: All authors have completed the ICMJE uniform disclosure form (available at https://qims.amegroups.com/article/view/10.21037/qims-22-1319/coif). The authors have no conflicts of interest to declare.

Ethical Statement: The authors are accountable for all aspects of the work in ensuring that questions related to the accuracy or integrity of any part of the work are appropriately investigated and resolved. This study does not involve humans or animals, ethical approval and written informed consent were not necessary for this review.

References

1. Joo CK, Shin JA, Kim JH. Capsular opening contraction after continuous curvilinear capsulorhexis and intraocular lens implantation. J Cataract Refract Surg 1996;22:585-90.
2. Dong J, Wang X, Wang X, Li J. A practical continuous curvilinear capsulorhexis self-training system. Indian J Ophthalmol 2021;69:2678-86.
3. Sharma B, Abell RG, Arora T, Antony T, Vajpayee RB. Techniques of anterior capsulotomy in cataract surgery. Indian J Ophthalmol 2019;67:450-60.

4. Bang SP, Jun JH. Comparison of postoperative axial stability of intraocular lens and capsulotomy parameters between precision pulse capsulotomy and continuous curvilinear capsulotomy: A prospective cohort study. Medicine (Baltimore) 2019;98:e18224.
5. Li S, Li X, He S, Zheng Q, Chen X, Wu X, Xu W. Early Postoperative Rotational stability and its related factors of a single-piece acrylic toric intraocular lens. Eye (Lond) 2020;34:474-9.
6. Li S, Hu Y, Guo R, Shao Y, Zhao J, Zhang J, Wang J. The effects of different shapes of capsulorrhexis on postoperative refractive outcomes and the effective position of the intraocular lens in cataract surgery. BMC Ophthalmol 2019;19:59.
7. Hu WF, Chen SH. Advances in capsulorhexis. Curr Opin Ophthalmol 2019;30:19-24.
8. Wang X, Dong J, Deng M. Limbus-centered marking technique-assisted continuous circular capsulorhexis. Medicine (Baltimore) 2021;100:e24109.
9. Lee JH, Lee YE, Joo CK. Clinical results of the open ring PMMA guider assisted capsulorrhexis in cataract surgery. BMC Ophthalmol 2018;18:116.
10. Naik MP, Sethi H, Kasiviswanathan P. Modified bandage-contact-lens used as a guide-marker for performing continuous-curvilinear-capsulorhexis by a first-year-post-graduate-ophthalmology-resident. Am J Ophthalmol Case Rep 2020;20:100889.
11. Dharampal, Mutneja V. Methods of Image Edge Detection: A Review. Journal of Electrical & Electronic Systems 2015;4:150.
12. Sumathy G, Arokia Renjit J. Distance-Based Method used to Localize the Eyeball Effectively for Cerebral Palsy Rehabilitation. J Med Syst 2019;43:262.
13. Ahmed AS. Comparative study among Sobel, Prewitt and Canny edge detection operators used in image processing. Journal of Theoretical and Applied Information Technology 2018;96:6517-25.
14. Su B, Gong Y, Chen Y, Liu Y, Wang Z, Dai M, Zhuang Y, Liu W, Kuang S, Zong Y, Wang J, Yao W. Detection of Healthy and Diseased Pylorus Natural Anatomical Center with Convolutional Neural Network Classification and Filters. J Med Biol Eng 2022;42:216-224.
15. Vincent OR, Folorunso O. A descriptive algorithm for Sobel image edge detection. Proceedings of informing science & IT education conference (InSITE), 2009:97-107.
16. Gao W, Zhang X, Yang L, Liu H. An Improved Sobel Edge Detection. 2010 3rd International Conference on Computer Science and Information Technology, 2010:67-71.
17. Tang X, Wang X, Hou J, Wu HF, Liu D. An Improved Sobel Face Gray Image Edge Detection Algorithm. 2020 39th Chinese Control Conference (CCC), 2020:6639-43.
18. Vinista P, Joe MM. A Novel Modified Sobel Algorithm for Better Edge Detection of Various Images. International Journal of Emerging Technologies in Engineering Research (IJETER) 2019;7:25-31.
19. Sridhar B. Investigations of Medical Image Segmentation Methods with Inclusion Mathematical Morphological Operations. Traitement du Signal 2021;38:1531-40.
20. Yusef YN, Vvedenskiy AS, Alhumidi K, Fokina ND, Demidov AL. Surgical treatment of hypermature cataract in patients with lens subluxation and small pupil. Vestn Oftalmol 2021;137:175-80.
21. Cheng L, Fang J, Wu Y, Kang K. Research on Improved Image Edge Detection Based on Hough Transform. Proc. SPIE 11928, International Conference on Image Processing and Intelligent Control (IPIC 2021), 2021:119280O.
22. S V MK, R G. Computer-Aided Diagnosis of Anterior Segment Eye Abnormalities using Visible Wavelength Image Analysis Based Machine Learning. J Med Syst 2018;42:128.

Cite this article as: Li Y, Wang X, Gong Q, Deng M, Chen S, Chen H. Ridge operator-assisted delineation of capsulorhexis border for cataract surgery. Quant Imaging Med Surg 2023;13(8):5119-5129. doi: 10.21037/qims-22-1319

